Turk J Pharm Sci 2024;21(2):113-124
DOI: 10.4274/tjps.galenos.2023.46095

ORIGINAL ARTICLE

Electrochemical Properties of Fused Pyrimidine-Triazole Heterocyclic Molecules as Novel Drug Candidates

Fatma KURUL[1]*, Hüseyin İSTANBULLU[2], Hüseyin Oğuzhan KAYA[3], Arif Engin ÇETİN[4], Seda Nur TOPKAYA[3]

[1]Dokuz Eylül University, İzmir International Biomedicine and Genome Institute, İzmir, Türkiye
[2]İzmir Katip Çelebi University Faculty of Pharmacy, Department of Pharmaceutical Chemistry, İzmir, Türkiye
[3]İzmir Katip Çelebi University Faculty of Pharmacy, Department of Analytical Chemistry İzmir, Türkiye
[4]İzmir Biomedicine and Genome Center, İzmir, Türkiye

ABSTRACT

Objectives: Triazolopyrimidinones are compounds used in medicinal chemistry. In this study, three novel triazolopyrimidinone derivatives were synthesized as drug candidates: (5-(chloromethyl)-2-(4-methoxyphenyl)-[1,2,4]triazolo[1,5-a]pyrimidin-7(3H)-one) (S1-TP), 2-(4-methoxyphenyl)-5-(piperidinomethyl)-[1,2,4]triazolo[1,5-a]pyrimidin-7(3H)-one) (S2-TP), and 2-(4-methoxyphenyl)-5-(morpholinomethyl)-[1,2,4]triazolo[1,5-a] pyrimidin-7(3H)-one) (S3-TP). Their electrochemical properties were investigated for the first time using voltammetric techniques on carbon graphite electrodes. Moreover, stability tests for each drug candidate were performed on different days. After revealing the electrochemical properties of the drug candidates, their effect on double-stranded (ds) DNA was examined by measuring the oxidation currents of the guanine of dsDNA before and after the interaction.

Materials and Methods: An electrochemical setup that included a pencil graphite electrode as the working electrode, an Ag/AgCl reference electrode, and a platinum wire as the auxiliary electrode was used in this study. Experiments for optimum pH, scan rate, and concentration of drug candidates were conducted. The interaction between Ss-TP and dsDNA was evaluated using differential pulse voltammetry. The stability of each drug candidate was tested on various days.

Results: A comprehensive characterization of the S1-TP, S2-TP, and S3-TP compounds was performed for the first time. This study showed that the electrochemical oxidation of S1-TP and S2-TP was irreversible and diffusion-controlled. In addition, the transfer of electrons in S3-TP was controlled by adsorption. The interaction between Ss-TP and dsDNA resulted in notable changes in the peak potentialof dsDNA. The dsDNA peak potential shifted negatively after interaction with S1-TP, S2-TP, and S3-TP. Under optimum conditions, the detection limits for S1-TP, S2-TP, and S3-TP were 1.5 µg/mL, 1.0 µg/mL, and 2.0 µg/mL, respectively.

Conclusion: From our experimental data, we concluded that these molecules can be used as drug molecules because of their remarkable effects on DNA.

Keywords: Drug candidate, drug, DNA, drug-DNA interaction, triazolopyrimidinone, heterocyclic compounds

INTRODUCTION

Triazolopyrimidinones, a class of fuzed pyrimidinone-triazole heterocyclic ring systems, are considered to be privileged scaffolds in medicinal chemistry. A wide range of bioactivities of triazolopyrimidinone-bearing compounds has been reported as FABPs, ferrochelatase, and per-arnt-sim kinase inhibitors.[1,2] In addition, triazolopyrimidinones and triazolopyrimidines with purine bioisosteric analogs have been reported to have anticancer activity through various mechanisms.[3] Fandzloch et al.[4] reported that triazolopyrimidine ruthenium (II) complexes show anticancer activity on various cancer cell lines, and these complexes bind to the minor groove of DNA or intercalate it.

*Correspondence: sedanur6@gmail.com, Phone: +90 507 444 16 07, ORCID-ID: orcid.org/0000-0002-7816-3155
Received: 14.02.2023, Accepted: 13.05.2023

Copyright© 2024 The Author. Published by Galenos Publishing House on behalf of Turkish Pharmacists' Association.
This is an open access article under the Creative Commons Attribution-NonCommercial-NoDerivatives 4.0 (CC BY-NC-ND) International License.

In another study, triazolopyrimidine copper (II) complexes and their DNA intercalating capacity were analyzed using absorption and fluorescence spectra.[5] The results suggested that the complexes were intercalated into DNA strands and damaged through metallonuclease activity. Harrison et al.[6] discovered a selective and highly soluble triazolopyrimidine derivative molecule as an NLRP3 inflammasome inhibitor using *an in silico* pharmacophore model, which could be used as an inhibitor for the treatment of inflammatory diseases.

Drugs and drug candidates can interact with DNA in several ways, and the interaction between them can be determined using various instrumental methods such as circular dichroism (CD), nuclear magnetic resonance (NMR), fourier transform infrared spectroscopy (FTIR), viscosity measurements, infrared spectroscopy (IR), mass spectrometry (MS), molecular docking, and electrochemical methods.[7-15] Morawska et al.[11] developed a voltammetric method to observe the electrochemical behavior of tenofovir and its interaction mechanism with ds/ssDNA and compared their method with spectrophotometric analyses, where the electrochemical method showed better analytical performance compared with spectrophotometry in terms of limit of detection (LOD) and linear range. In another study, the interaction mechanism of mitoxantrones and DNA molecules was studied using FTIR, ultraviolet-visible spectroscopy (VIS), and CD. According to spectroscopic results, mitoxantrone possibly binds to DNA from guanine (N7), thymine (O2), and cytosine (O2) locations.[16] Electrochemical methods are preferred because of their rapidness, high selectivity, low instrumentation cost, simple operation, and portability. They could reveal the chemical properties and potential toxic effects of drug candidates and determine the metabolic processes.[17]

The main interaction modes between the drug molecules and DNA can be simply classified as covalent and non-covalent binding. Among them, covalent binding with DNA is irreversible, inhibits the functions of DNA, and leads to cell death. In contrast, non-covalent binding is reversible, and they are subclassified as electrostatic, groove, and intercalative bindings. Electrostatic binding results from the interactions of positively charged ligands with the negatively charged DNA phosphate backbone structure. Groove binding is also sub-categorized as minor and major groove binding in which small ligands bind to the minor or major groove of DNA by van der Waals or hydrogen bonds. Small ligands can bind to DNA *via* unique binding sites, and this mode is called intercalation. In this mode, intercalators containing planar heterocycle groups could slide and stack between base pairs of DNA and stabilize the duplex without breaking the base pair or forming covalent bonds.

Our study is the first to analyze the electrochemical properties of novel triazolopyrimidine derivatives as purine analog chemical structures. First, we investigated the electrochemical properties of novel drug candidates, and then their interaction with dsDNA was analyzed using voltametric methods as differential pulse voltammetry (DPV) and cyclic voltammetry (CV). Experimental parameters, *e.g.*, pH, concentration of drug candidates, and scan rate, were examined to reveal the analytical properties of these novel drug candidates. Stability tests were performed under optimal storage conditions and within different days to observe the shelf life of the drug candidates.

MATERIALS AND METHODS

Materials

Salmon sperm DNA used in this experiment (Sigma Aldrich, purity ≥ 98%) was dissolved in deionized water to prepare stock solutions. 3-Amino-5-(methylthio)-4H-1,2,4-triazole (Merck, purity ≥ 97%) and chloroform (Alfa Aesar-Acros Organics, purity ≥ 99%) were used as received without further purification. The buffers were prepared using analytical grade chemicals from various companies such as Carlo Erba, Alfa Thermo Fisher Scientific, and Isolab. In the experiments, we used 0.5 M acetate (ACB, pH: 3.8, 4.8, 5.6) and 0.05 M phosphate (PBS, pH: 7.4) buffers containing 0.02 M NaCl and 0.05 M Tris-EDTA (TE, pH: 8.0) buffer.

Instrumentation

Analytical thin layer chromatography (TLC) was performed using Merck silica gel F-254 plates. Melting points were employed with Stuart SMP 30 (Staffordshire, ST15 OSA). NMR spectra were reported with a Varian AS 400 Mercury plus NMR (Varian Inc.) spectrometer at 400 MHz for ^{1}H and 100 MHz for ^{13}C using DMSO-*d6* as the solvent. The coupling constants (J) are presented in Hertz (Hz) without an internal standard. Splitting patterns were designated as follows: s (singlet); d (doublet); t (triplet); p (pentet); and m (multiplet). HR-MS was performed on Agilent 6200 Series TOF and 6500 Series Q-TOF LC/MS System with ESI (+) ionization. Microwave irradiation (MW) synthesis of the compounds was conducted on a Milestone MicroSYNTH (Milestone S.r.l.) microwave apparatus. A PalmSens4 handheld analyzer with PSTrace 5.8 software was used in electrochemical studies. Pencil graphite electrodes were employed as the working electrodes. To complete the three-electrode system, a platinum wire and an Ag/AgCl electrode were employed as auxiliary and reference electrodes, respectively.

Experimental

General synthesis of the drug candidates

The synthesis steps are shown in Figure 1.

Synthesis of the substituted triazole

5-(4-Metoxyphenyl)-3-amino-1,2,4-triazole was synthesized according to reference.[18] In the first step, aminoguanidine bicarbonate and 4-metoxybenzoyl chloride reacted. Later, the amide derivative was cyclized to yield 5-(4-metoxyphenyl)3-aminotriazole.

Synthesis of S_1-TP

5-(4-Metoxyphenyl)-3-amino-1,2,4-triazole (10 mmol) and ethyl 4-chloroacetoacetate (20 mmol) were mixed in 18 mL acetic acid (MW, 20 min, 180 °C). The formed solid was filtered, rinsed with acetic acid, and dried. These steps yielded S_1-TP (5-(chloromethyl)-2-(4-methoxyphenyl)-[1,2,4]triazolo[1,5-*a]* pyrimidin-7(*3H*)-one, which was used in the next steps without purification.

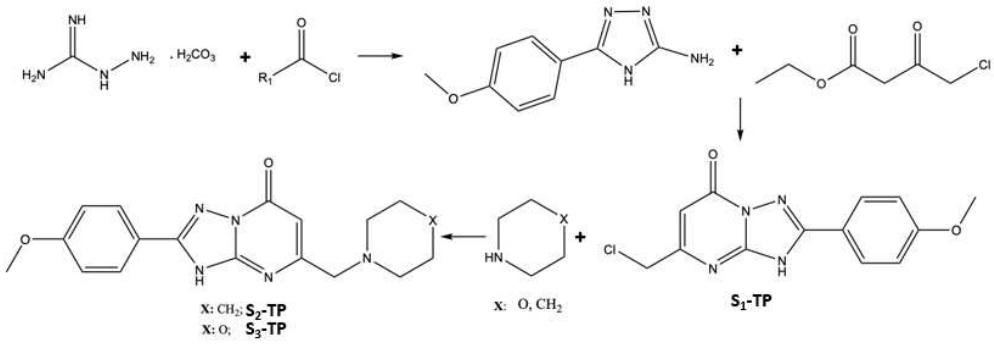

Figure 1. General synthesis scheme of the pyrimidinone-triazole derivatives: S_1-TP, S_2-TP, and S_3-TP
The characterization results are presented in the Supplementary Information (Supplementary Figures 1-6, Data Sheets 1-3)

Synthesis of S_2-TP and S_3-TP

In the last step of the synthesis, the nucleophilic substitution of the obtained S_1-TP with piperidine and morpholine yielded S_2-TP and S_3-TP. S_1-TP (1 mmol) and amine derivatives, namely, piperidine/morpholine (2 mmol), were stirred in 16 mL dimethylformamide (DMF) in the presence of 1.5 mmol caesium carbonate (Cs_2CO_3) using MW irradiation (150 W, 15-30 min, 95 °C). The excess Cs_2CO_3 was filtered, and the filtrate was concentrated under reduced pressure. This mixture was further purified by column chromatography over silica gel 60 (70-230 mesh American Standard Test Sieve Series, Merck) with chloroform: methanol (10:2), and the compounds were recrystallized from methanol or acetone. The crude yield was 40-45%.

S_2-TP: 2-(4-Methoxyphenyl)-5-(piperidinomethyl)-[1,2,4]triazolo[1,5-*a*]pyrimidin-7(*3H*)-one

S_3-TP: 2-(4-Methoxyphenyl)-5-(morpholinomethyl)-[1,2,4]triazolo[1,5-*a*]pyrimidin-7(*3H*)-one

Electrochemical investigation of drug candidates

+ 1.4 V potential for 30 s was applied to activate and clean the PGEs. 1000 µg/mL was prepared with TE buffer and diluted with ACB. 1000 µg/mL) were prepared in DMF and diluted with appropriate buffers. These solutions were then added to the electrochemical measuring cell. Activated PGEs were dipped in these solutions, and DPV measurements were performed.

Interaction

Solutions containing 50 µg/mL of dsDNA and 10 µg/mL of drug candidates were mixed in ACB (pH: 3.8 for S_1-TP/DNA, S_2-TP/DNA; and pH: 5.6 for S_3-TP/DNA). The solutions were then placed in a thermal shaker at 600 rpm and 45 °C for 30 min. Then, 100 µL of this interaction solution was added to the tubes. The PGEs were immersed in the interaction solutions for 30 min. Then, DPV measurements were performed.

Measurement

DPV and CV measurements were performed from + 0.4 and + 1.4 V at a scan rate of 100 mV/s with 0.5 s interval time. The experimental steps are illustrated in Figure 2.

RESULTS AND DISCUSSION

Synthesis of the compounds

Three novel drug candidates were synthesized follows:

5-(Chloromethyl)-2-(4-methoxyphenyl)-[1,2,4]triazolo[1,5-a]pyrimidin-7(3H)-one (S1-TP)

Yellow solid; yield, 52 %; *m.p.*, 113 °C; ^{1}H-NMR (DMSO-d_6, 400 MHz) δ 8.02 (d, *J*= 8.7 Hz, 2H), 7.07 (d, *J*= 8.8 Hz, 2H), 6.16 (s, 1H), 4.66 (s, 2H), 3.81 (s, 3H) ppm; ^{13}C-NMR (DMSO-d_6, 100 MHz) δ 161.6, 156.1, 151.8, 128.7, 114.8, 100.4, 55.8ppm; $C_{13}H_{11}ClN_4O_2$ HRMS *m/z*: 290.0552 (Calcd for 290.05705)

2-(4-Methoxyphenyl)-5-(piperidinomethyl)-[1,2,4]triazolo[1,5-a]pyrimidin-7(3H)-one (S2-TP)

Yellow solid; yield, 30 %; *m.p.*, 128 °C; ^{1}H-NMR (DMSO-d_6, 400 MHz) δ 8.01 (d, *J*= 8.7 Hz, 2H), 6.99 (d, *J*= 8.8 Hz, 2H), 5.63 (s, 1H), 3.79 (s, 3H), 3.30 (s, 2H), 3.23 (s, 2H), 2.34-2.42 (m, 2H), 1.50 (p, *J*= 5.5 Hz, 4H), 1.34-1.43 (m, 2H) ppm; ^{13}C-NMR (DMSO-d_6, 100 MHz) δ 162.39, 160.28, 159.72, 158.74, 128.12, 125.96, 114.21, 94.35, 65.34, 55.59, 54.70, 26.19, 24.47 ppm; $C_{18}H_{21}N_5O_2$ HRMS *m/z*: 339.16979 (Calcd for 339.16952).

2-(4-Methoxyphenyl)-5-(morpholinomethyl)-[1,2,4]triazolo[1,5-a]pyrimidin-7(3H)-one (S3-TP)

Yellow solid; yield, 35 %; *m.p.*, 103 °C; ^{1}H-NMR (DMSO-d_6, 400 MHz) δ 8.02 (d, *J*= 8.9 Hz, 2H), 6.99 (d, *J*= 8.9 Hz, 2H), 5.66 (s,

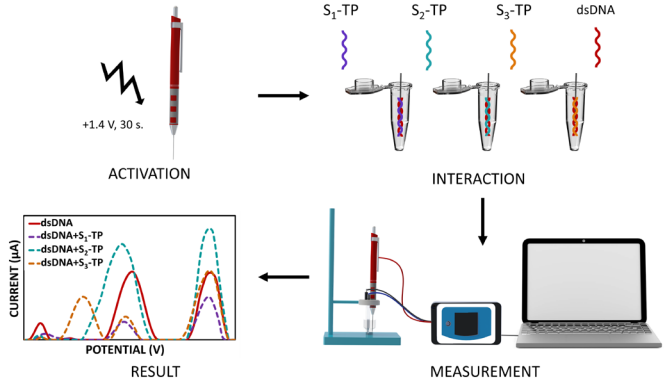

Figure 2. Experimental steps: activation of PGE with ACB, interaction of dsDNA with S_1-TP, S_2-TP, and S_3-TP, and DPV measurements
DPV: Differential pulse voltammetry, dsDNA: Double-stranded DNA

1H), 3.79 (s, 3H), 3.53-3.65 (m, 4H), 3.28 (s, 2H), 2.37-2.47 (m, 4H) ppm; ^{13}C-NMR (DMSO-d_6, 100 MHz) δ 161.27, 160.51, 160.34, 159.55, 158.65, 128.16, 125.82, 114.23, 94.76, 66.76, 64.72, 55.59, 53.91 ppm; $C_{17}H_{19}N_5O_3$ HRMS *m/z*: 341.14814 (Calcd for 341.14879).

The designed compounds were synthesized in three steps (Figure 1). The structures of the final compounds were determined by spectral analyses the spectroscopic data confirmed the proposed structures. In the ^{1}H NMR spectra, the hydrogen atom of the heterocyclic ring was observed as a singlet signal between δ 5.63-6.16 ppm. The methylene protons, attached to the heterocyclic ring at 5 positions, were observed as singlets with two proton integrals between δ 4.66-3.28 ppm. The proton signals of the benzene ring and cyclic amines were identified in the expected chemical shifts with expected divisions. The observed carbon signals in the ^{13}C NMR of the compounds were in accordance with those of the target compounds. The amide carbon signal was observed between δ 161-162 ppm in ^{13}C NMR spectrums.

The purity of the compounds was determined using HRMS spectra. The HRMS data were in accordance with the molecular formula and a found value within 0.003 *m/z* unit of the calculated value of a parent-derived ion. S_2-TP and S_3-TP were introduced earlier in the literature,[19] while the full spectral characterization of these compounds was introduced in this article.

Electrochemical properties of the drug candidates

In this section, the electrochemical behaviors of the drug candidates were analyzed using DPV. Because pH is important for the metabolism of drug molecules, the effect of pH on the oxidation signals of drug candidates was examined, and the obtained results are shown in Figure 3.

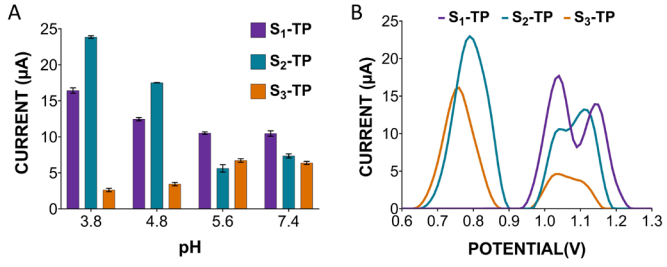

Figure 3. (A) Effect of pH on peak currents. Bar graphs: drug candidates at different pH values, 3.8 to 7.4, (B) DPV voltammogram of S_1-TP, S_2-TP, and S_3-TP prepared in ACB (pH: 3.8 for S_1-TP and S_2-TP, and pH: 5.6 for S_3-TP
DPV: Differential pulse voltammetry

For the pH study in DPV, drug candidates were prepared using buffers with pH ranging from 3.8 to 7.4. As shown in Figure 3A, S_1-TP and S_2-TP produced stable responses, and the highest currents were obtained at pH 3.8. S_3-TP showed the highest electrochemical signal at pH 5.6. Thus, pH 5.6 was chosen as the dilution buffer for S_3-TP (Figure 3A).

At pH 3.8, the oxidation peak potentials of S_1-TP were detected at 1.03 V and 1.15 V. Because it is more stable and higher, the signal obtained at 1.03 V was chosen as the main oxidation signal for further studies. At pH 3.8, S_2-TP produced two oxidation signals at 0.79 V and 1.11 V. At pH 5.6, the oxidation peak potentials of S_3-TP were observed at 0.76 V and 1.04 V (Figure 3B). All oxidation signals shifted to lower potentials with pH. These shifts in the peak potentials of drugs demonstrate that protons participate in the oxidation process of drugs.[20]

As shown in Figure 3B, all the drug candidates have oxidation capacity. The triazolopyrimidinone structure could form triazolopyrimidine by H atom shifting and tautomerization. Several factors could contribute to the stability between the two tautomers, *e.g.*, substitution, aromaticity, hydrogen bonding, and solvation. The redox mechanism of these novel agents on graphite electrode surfaces could involve the oxidation of the phenol groups of the compounds. Heteroatoms in the substituted amines might also contribute to the oxidation potency of the compounds, *e.g.*, they could change the oxidation potency. Considering the phenolic tautomerization of the heteroaromatic ring and the amine substitution, the title compound could possess oxidative properties.

In the second part of our study, DPV measurements were performed at different concentrations of drug candidates at 100 mV/s to determine the analytical concentration ranges for the drug candidates (Figure 4).

The formulas for calculating the LOD and limit of quantification (LOQ) depend on the specific method used, but generally, the LOD is calculated as 3 times the standard deviation of the response (ss) divided by the slope of the calibration curve (m), while the LOQ is calculated as 10 times the standard deviation of the response divided by the slope of the calibration curve'.

LOD = 3 s/m

LOQ = 10 s/m

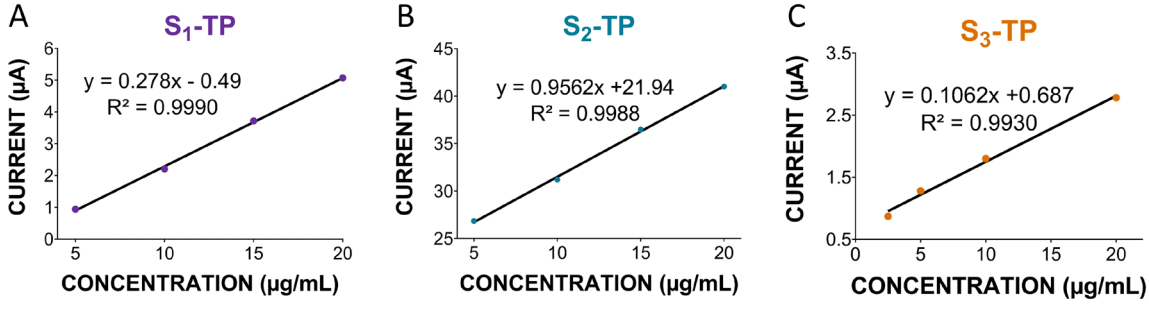

Figure 4. Calibration graphs for (A) S_1-TP, (B) S_2-TP, and (C) S_3-TP obtained from drug concentration *vs.* current peak data

LOD and LOQ were determined from Figure 4. For S_1-TP and S_2-TP, LOD and LOQ were calculated from the concentrations 5, 10, 15, and 20 µg/mL. For S_3-TP, LOD and LOQ were calculated from the concentrations 2.5, 5, 10, and 20 µg/mL. LOD and LOQ for S_1-TP are 1.5 µg/mL and 5.0 µg/mL, respectively (Figure 4A). The LOD and LOQ for S_2-TP are 1.0 µg/mL and 3.4 µg/mL, respectively (Figure 4B). The LOD and LOQ for S_3-TP are 2.0 µg/mL and 6.8 µg/mL, respectively (Figure 4C). The correlation coefficients were 0.9990, 0.9988, and 0.9930 for S_1-TP, S_2-TP, and S_3-TP, respectively.

The effects of scan rate (V) on peak current (I_p) were studied using a CV between 25 and 150 mV/s, as shown in Figure 5.

As shown in Figure 5A, the anodic peak current (Ip_a) has a linear relationship with the scan rate (v):

S_1-TP: Ip_a (µA) = 0.374v + 17.666 (R^2= 0.9990) (Equation 1)

S_2-TP: Ip_a (µA) = 0.1316v + 6.2628 (R^2= 0.9880) (Equation 2)

S_3-TP: (µA) = 0.2254v + 2.2687 (R^2= 0.9980) (Equation 3)

As shown in Figure 5B, the peak current (Ip_a) also has a linear relationship with the root of the scan rate ($v^{1/2}$):

S_1-TP: Ip_a (µA) = 203.97$v^{(1/2)}$ – 7.7443 (R^2=0.9928) (Equation 4)

S_2-TP: Ip_a (µA) = 72.771$v^{(1/2)}$ – 2.9923 (R^2=0.9977) (Equation 5)

S_3-TP: Ip_a (µA) = 122.95$v^{(1/2)}$ – 13.05 (R^2=0.9920) (Equation 6)

In Figure 5C, log(Ip_a) and log(v) linear relationship is presented within the scan rate range between 25 and 150 mV/s:

S_1-TP: *log* Ip_a = 0.5716 *log* v + 2.3213 (R^2=0.9937) *(Equation 7)*

S_2-TP: *log* Ip_a = 0.5996 *log* v + 1.899 (R^2= 0.9987) *(Equation 8)*

S_3-TP: *log* Ip_a = 0.8568 *log* v + 2.2551 (R^2= 0.9978) *(Equation 9)*

According to the literature, these slope values are close to the theoretical value, *e.g.*, 0.5, indicating diffusion-controlled processes, whereas for the theoretical value 1, the process is adsorption-controlled.[21] The slopes of Equations 7 and 8 were determined to be 0.5716 and 0.5996, respectively, which indicates that electrochemical oxidation of S_1-TP and S_2-TP are diffusion-controlled processes. According to Equation 9, the slope is 0.8568, which proves that the electrode process was adsorption controlled for S_3-TP.

Interaction

The intrinsic electroactivity of adenine and guanine bases is generally used as an indicator of drug-DNA interactions. In the next step of our study, we studied the interaction of drug candidates with dsDNA. 100 µg/mL were prepared with TE buffer (pH: 8.0).

The stock drug solutions were prepared with DMF and diluted with ACB (pH: 3.8 for S_1-TP and S_2-TP, and pH: 5.6 for S_3-TP). The final concentrations of dsDNA and Ss-TP were 50 µg/mL and 10 µg/mL, respectively. All solutions were placed in a thermal shaker, where stirring was applied at 600 rpm and 45 °C for 30 min. Then, 100 µL of the solution was transferred into tubes, and the electrodes were immersed in these tubes for 30 min. Oxidation signals were measured with DPV in the range between 0 and 1.4 V at a scan rate of 50 mV/s in the absence and presence of drug candidate molecules. Analytical signals associated with the guanine bases of DNA were obtained at ~1.0 V *vs.* Ag/AgCl.

In Figure 6A, two distinct oxidation signals associated with dsDNA in ACB (pH: 3.8) were obtained at + 0.92 V and + 1.17

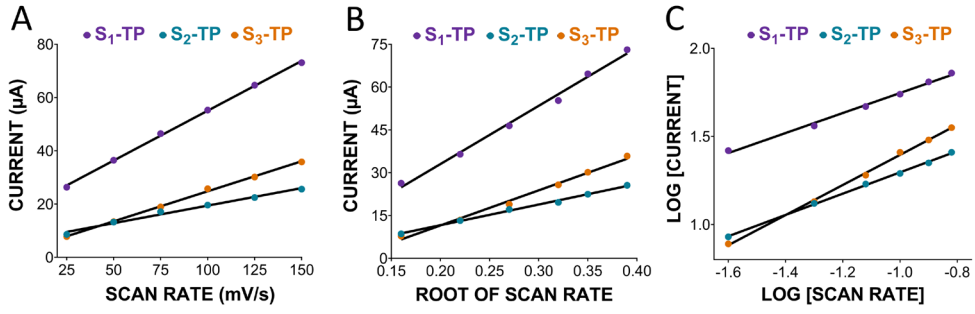

Figure 5. Effect of (A) scan rate and (B) scan rate root on peak current, and (C) scan rate on the log of peak current

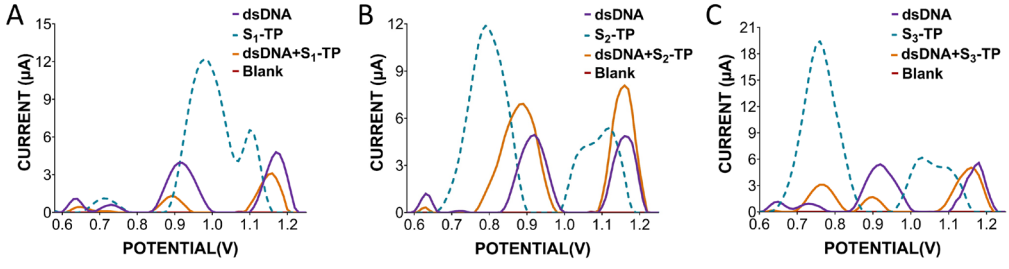

Figure 6. Differential pulse voltammograms of the guanine oxidation currents of dsDNA after interaction with (A) S_1-TP, (B) S_2-TP, and (C) S_3-TP. The experimental steps were as follows: PGE pretreatment: 1.4 V for 30 s, interaction: 100 µg/mL of dsDNA and 20 µg/mL of drug candidates, stirring: 600 rpm at 45 °C for 30 min, adsorption: 30 min, and DPV measurement within a range between 0 and + 1.4 V at 50 mV/s in ACB

dsDNA: Double-stranded DNA, DPV: Differential pulse voltammetry

V. After interaction with S_1-TP, the peak potential of dsDNA shifted to + 0.89 V and + 1.16 V, respectively. On the other hand, after interaction with S_2-TP, one of the peak potentials of dsDNA shifted negatively from + 0.92 V to + 0.89 V. Oxidation signals of dsDNA in ACB (pH: 5.6) were obtained at + 0.92 V and + 1.18 V. In the presence of S_3-TP, the peak potentials of dsDNA slightly shifted toward smaller values, *e.g.*, + 0.90 V and + 1.16 V (Figure 6C). dsDNA oxidation potentials shifted negatively after interacting with S_1-TP, S_2-TP, and S_3-TP. Here, positive or negative shifts in peak potential can reveal the interaction mechanism between the drug candidate and dsDNA. Positive peak potential shifts are associated with intercalative binding, whereas negative peak potential shifts are associated with electrostatic binding.[22] Bilge et al.[23] reported the interaction mechanism between ibrutinib (IBR) and dsDNA using electrochemical and molecular docking techniques. Voltametric studies have indicated that the peak potential of IBR shifts toward less positive potentials because of electrostatic interaction.[23] In our study, the shift in the peak potential toward negative could be attributed to the irreversible electrode process.[24] The reason for this shift could be explained by the electrostatic binding between Ss-TP and dsDNA.

In Figure 6A, the peak currents of dsDNA were found as 3.95 µA and 4.79 µA with the relative standard deviation (RSD) 5.45%, 3.76% which decreased to 1.30 µA and 3.11 µA after the interaction with RSD 3.12%, 4.87% (n= 5). In Figure 6B, the peak currents of dsDNA were found as 4.94 µA and 4.86 µA with RSD 1.68% and 4.54%, respectively, which increased, *e.g.*, 6.92 µA with RSD 3.95% and 7.62% and 8.08 µA with RSD 1.49% and 5.23%, due to the binding of S_2-TP to dsDNA, changing the dsDNA structure. Figure 6C demonstrates that S_3-TP caused a significant change in the oxidation currents of dsDNA. Here, the peak currents of dsDNA are as 5.42 µA with RSD 2.97% and 5.58 µA with RSD 7. 66%, while after interaction, we determined three peaks at 3.07 µA with RSD 5.22%, 1.66 µA with RSD 9.13%, and 5.03 µA with RSD 4.68%.

Stability

Stability is one of the most important factors related to the efficacy of drug candidates. To evaluate the stability of the drug candidates, we performed DPV (Figure 7). Stock solutions of drug candidates were freshly prepared and stored in the dark at room temperature (25 °C). Stock solutions of drug candidates measured within 0, 5, 7, 14, and 30 days. Here, S_1-TP and S_3-TP exhibited good stability for 30 days of storage without significant percentage changes in current values, *e.g.*, we observed a slight reduction in the percentage of current for S_1-TP between days 0 and 30. At the end of day 30, the percentage of the current values for S_1-TP was determined to be 91%. A noticeable change in the percentage current of S_2-TP was observed on day 30, *i.e.*, 48%. In contrast, minute changes in the current values of S_2-TP were observed between days 7 and 30, *e.g.*, the current value of S_3-TP decreased to 86% at day 30. These results proved that the stock solutions of drugs were stable for 30 days, except S_2-TP, which could be very advantageous for long-term use by retaining their pharmaceutical properties.

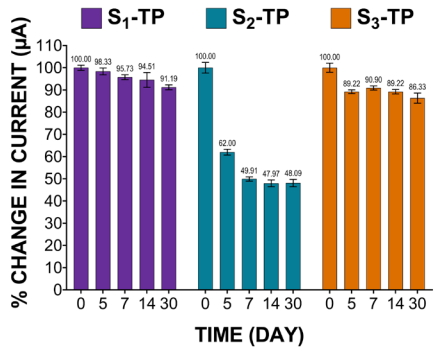

Figure 7. Change in current for S_1-TP, S_2-TP, and S_3-TP examined at 25 °C on different days, *e.g.*, 0, 5, 7, 14, and 30. The percentage current values of drug candidates were 91%, 48%, and 86% by the end of 30 days, respectively

CONCLUSION

In conclusion, in this article, we for the first time studied the full characterization of S_1-TP, S_2-TP, and S_3-TP compounds. Importantly, S_1-TP is reported for the first time in the literature, whereas S_2-TP and S_3-TP compounds were reported in the literature only for their screening activity against FABPs (Patent no; WO 2010/056630 A1). We have introduced the synthetic pathway and full spectral characterization data of these compounds to the literature. Our study focused on the electrochemical behaviors of Ss-TP and their interactions with dsDNA using DPV and CV. We showed that the interaction of Ss-TP-dsDNA resulted in significant changes in the dsDNA peak potential. The dsDNA peak potential shifted negatively after interaction with S_1-TP, S_2-TP, and S_3-TP. The shift of the dsDNA peak potential reveals the interaction of Ss-TP with DNA supporting the binding in between. Moreover, the shift in the peak potential of dsDNA toward more positive values indicates that the DNA-drug interaction mechanism is intercalation, whereas the shift toward more negative values indicates that the DNA-drug interaction mechanism is an electrostatic mode. Our study also showed that the electrochemical oxidation processes of S_1-TP and S_2-TP were irreversible and controlled by diffusion. In addition, the electron transfer process was an adsorption-controlled process for S_3-TP. We believe our study can provide critical information for understanding the DNA-drug interaction, which could be very advantageous for analyzing new drug compounds and their potential effects on target biomolecules.

Ethics

Ethics Committee Approval: This study does not require any ethical permission.

Informed Consent: Not necessary.

Authorship Contributions

Concept: H.O.K., H.İ., S.N.T., Design: F.K, H.O.K., H.İ., S.N.T., Data Collection or Processing: F.K., H.O.K., H.İ., A.E.Ç., S.N.T, Analysis or Interpretation: F.K., H.O.K., H.İ., A.E.Ç., S.N.T., Literature Search: F.K., H.O.K., H.İ., A.E.Ç., S.N.T., Writing: F.K., H.O.K., H.İ., A.E.Ç., S.N.T.

Conflict of Interest: No conflict of interest was declared by the authors.

Financial Disclosure: The authors declared that this study received no financial support.

REFERENCES

1. Aggarwal R, Sumran G. An insight on medicinal attributes of 1,2,4-triazoles. Eur J Med Chem. 2020;205:112652.
2. Janganati V, Ponder J, Balasubramaniam M, Bhat-Nakshatri P, Bar EE, Nakshatri H, Jordan CT, Crooks PA. MMB triazole analogs are potent NF-κB inhibitors and anti-cancer agents against both hematological and solid tumor cells. Eur J Med Chem. 2018;157:562-581.
3. Huo JL, Wang S, Yuan XH, Yu B, Zhao W, Liu HM. Discovery of [1,2,4] triazolo[1,5-a]pyrimidines derivatives as potential anticancer agents. Eur J Med Chem. 2021;211:113108.
4. Fandzloch M, Jędrzejewski T, Dobrzańska L, Esteban-Parra GM, Wiśniewska J, Paneth A, Paneth P, Sitkowski J. New organometallic ruthenium(ii) complexes with purine analogs-a wide perspective on their biological application. Dalton Trans. 2021;50:5557-5573.
5. Ruta LL, Farcasanu IC, Bacalum M, Răileanu M, Rostas AM, Daniliuc C, Chifiriuc MC, Măruțescu L, Popa M, Badea M, Iorgulescu EE, Olar R. Biological activity of triazolopyrimidine copper(ii) complexes modulated by an auxiliary N-N-Chelating heterocycle ligands. Molecules. 2021;26:6772.
6. Harrison D, Bock MG, Doedens JR, Gabel CA, Holloway MK, Lewis A, Scanlon J, Sharpe A, Simpson ID, Smolak P, Wishart G, Watt AP. Discovery and optimization of triazolopyrimidinone derivatives as selective NLRP3 inflammasome inhibitors. ACS Med Chem Lett. 2022;13:1321-1328.
7. Beniaminov AD, Chashchina GV, Livshits MA, Kechko OI, Mitkevich VA, Mamaeva OK, Tevyashova AN, Shtil AA, Shchyolkina AK, Kaluzhny DN. Discrimination between G/C binding sites by olivomycin a is determined by kinetics of the drug-DNA interaction. Int J Mol Sci. 2020;21:5299.
8. Erol A, Akpınar F, Muti M. Electrochemical determination of anticancer drug bendamustine and its interaction with double strand DNA in the absence and presence of quercetin. Colloids Surf B Biointerfaces. 2021;205:111884.
9. Ijäs H, Shen B, Heuer-Jungemann A, Keller A, Kostiainen MA, Liedl T, Ihalainen JA, Linko V. Unraveling the interaction between doxorubicin and DNA origami nanostructures for customizable chemotherapeutic drug release. Nucleic Acids Res. 2021;49:3048-3062.
10. Kozieł SA, Lesiów MK, Wojtala D, Dyguda-Kazimierowicz E, Bieńko D, Komarnicka UK. Interaction between DNA, albumin and apo-transferrin and iridium(III) complexes with phosphines derived from fluoroquinolones as a potent anticancer drug. Pharmaceuticals (Basel). 2021;14:685.
11. Morawska K, Popławski T, Ciesielski W, Smarzewska S. Electrochemical and spectroscopic studies of the interaction of antiviral drug tenofovir with single and double stranded DNA. Bioelectrochemistry. 2018;123:227-232.
12. Nimal R, Nur Unal D, Erkmen C, Bozal-Palabiyik B, Siddiq M, Eren G, Shah A, Uslu B. Development of the electrochemical, spectroscopic and molecular docking approaches toward the investigation of interaction between DNA and anti-leukemic drug azacytidine. Bioelectrochemistry. 2022;146:108135.
13. Ponkarpagam S, Vennila KN, Elango KP. Molecular spectroscopic and molecular simulation studies on the interaction of oral contraceptive drug ormeloxifene with CT-DNA. Spectrochim Acta A Mol Biomol Spectrosc. 2022;278:121351.
14. Shahabadi N, Abbasi AR, Moshtkob A, Hadidi S. Design, synthesis and DNA interaction studies of new fluorescent platinum complex containing anti-HIV drug didanosine. J Biomol Struct Dyn. 2020;38:2837-2848.
15. Wang W, Zhang Y, Liu D, Zhang H, Wang X, Zhou Y. Prediction of DNA-binding protein-drug-binding sites using residue interaction networks and sequence feature. Front Bioeng Biotechnol. 2022;10:822392.
16. Agarwal S, Jangir DK, Mehrotra R. Spectroscopic studies of the effects of anticancer drug mitoxantrone interaction with calf-thymus DNA. J Photochem Photobiol B. 2013;120:177-182.
17. Diculescu VC, Chiorcea-Paquim AM, Oliveira-Brett AM. Applications of a DNA-electrochemical biosensor. TrAC Trends Anal Chem. 2016;79:23-36.
18. Istanbullu H, Bayraktar G, Ozturk I, Coban G, Saylam M. Design, synthesis and bioactivity studies of novel triazolopyrimidinone compounds. J Res Pharm. 2022;26:231-242.
19. Lengyel E, Nieman K, Kenny H. Methods for treating ovarian cancer by inhibiting fatty acid binding proteins. 2014.
20. Deng P, Xu Z, Kuang Y. Electrochemically reduced graphene oxide modified acetylene black paste electrode for the sensitive determination of bisphenol A. J Electroanal Chem. 2013;707:7-14.
21. Jakóbczyk P, Dettlaff A, Skowierzak G, Ossowski T, Ryl J, Bogdanowicz R. Enhanced stability of electrochemical performance of few-layer black phosphorus electrodes by noncovalent adsorption of 1,4-diamine-9,10-anthraquinone. Electrochim Acta. 2022;416:140290.
22. S Sirajuddin M, Ali S, Badshah A. Drug-DNA interactions and their study by UV-Visible, fluorescence spectroscopies and cyclic voltametry. J Photochem Photobiol B. 2013;124:1-19.
23. Bilge S, Dogan-Topal B, Taskin Tok T, Atici EB, Sınağ A, Ozkan SA. Investigation of the interaction between anticancer drug ibrutinib and double-stranded DNA by electrochemical and molecular docking techniques. Microchem J. 2022;180:107622.
24. Radi A, El Ries MA, Kandil S. Electrochemical study of the interaction of levofloxacin with DNA. Anal Chim Acta. 2003;495:61-67.

SUPPLEMENTARY INFORMATION

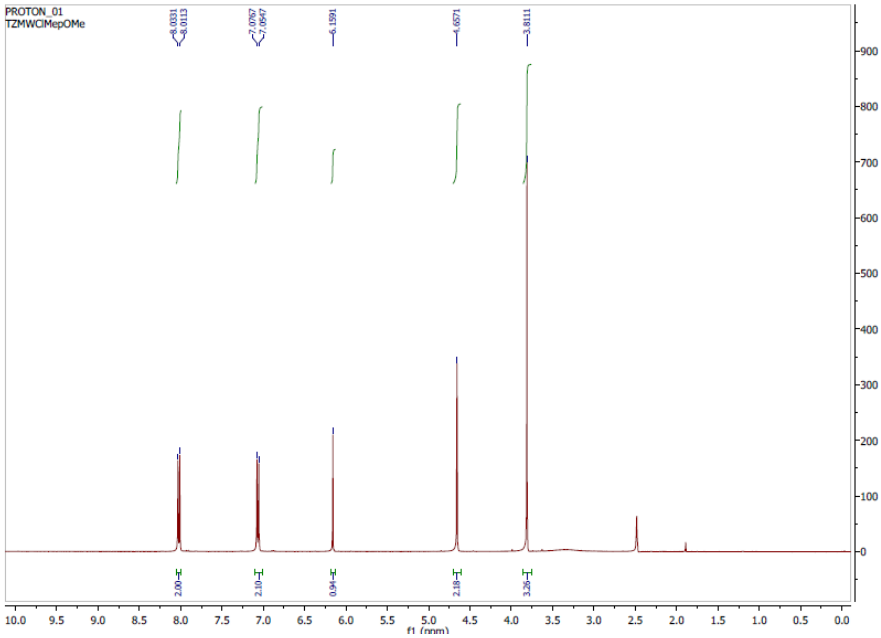

Supplementary Figure 1. ^{1}H NMR spectrum of S_1-TP.

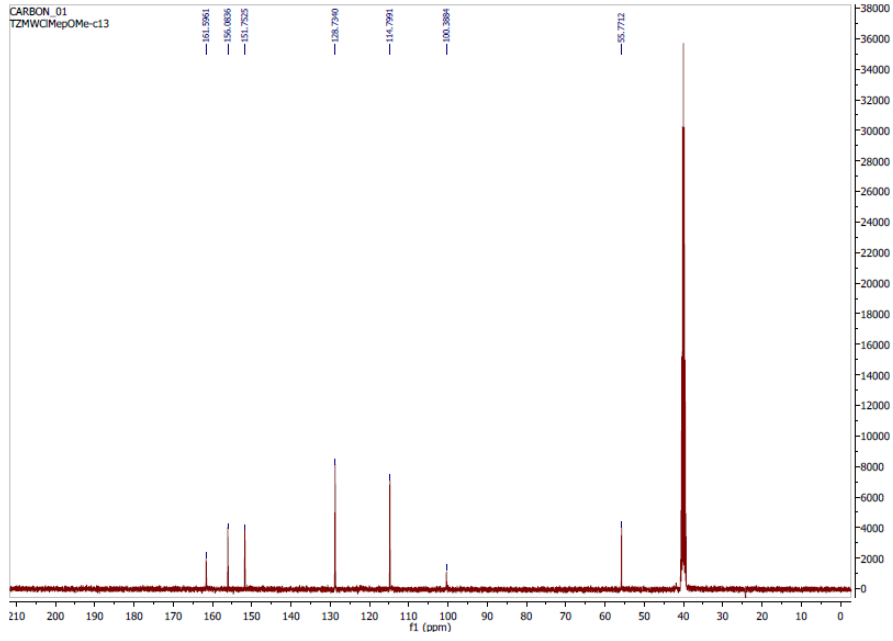

Supplementary Figure 2. ^{13}C NMR spectrum of S_1

User Spectra

Fragmentor Voltage	Collision Energy	Ionization Mode
90	0	ESI

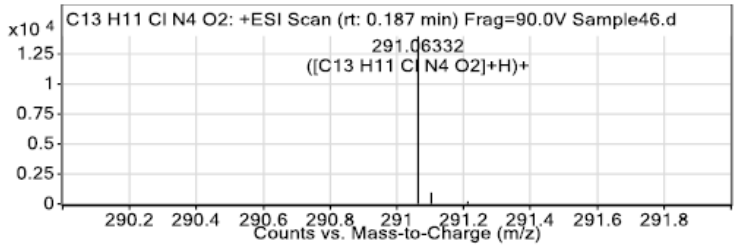

Peak List

m/z	z	Abund	Formula	Ion
291.06332	1	13984.74	C13 H11 Cl N4 O2	(M+H)+
313.04364	1	22951.55		
315.04157	1	6561.68		
329.01804	1	7036.92		
603.10071	1	101639.05		
604.10314	1	28659.66		
605.09877	1	67451.13		
606.09997	1	16867.94		
607.09646	1	11783.25		
619.07417	1	9988.45		

Formula Calculator Element Limits

Element	Min	Max
C	3	13
H	0	11
N	0	4
O	0	2
Cl	0	1

Formula Calculator Results

Formula	Best	Mass	Tgt Mass	Diff (ppm)	Ion Species	Score
C13 H11 Cl N4 O2	DOĞRU	290.05552	290.05705	5.29	C13 H12 Cl N4 O2	80.21

Data Sheet 1. HRMS data of S_1-TP

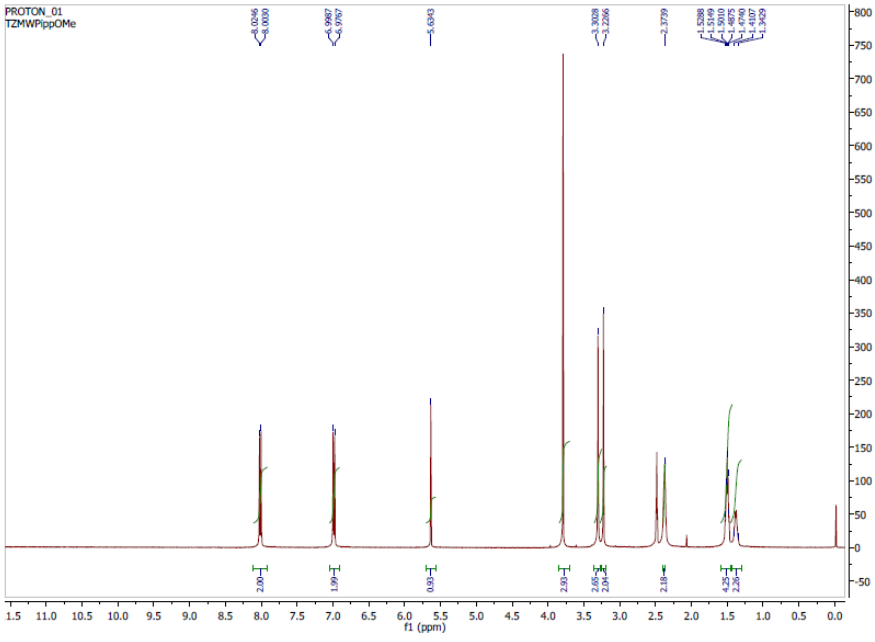

Supplementary Figure 3. ^{1}H NMR spectrum of S_2-TP

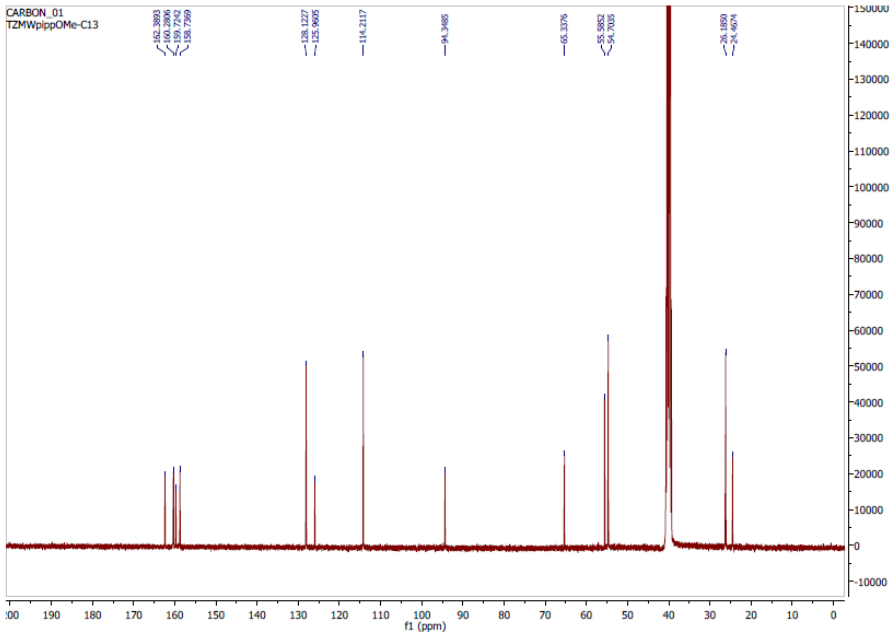

Supplementary Figure 4. ^{13}C NMR spectrum of S_2

User Spectra

Fragmentor Voltage	Collision Energy	Ionization Mode
90	0	ESI

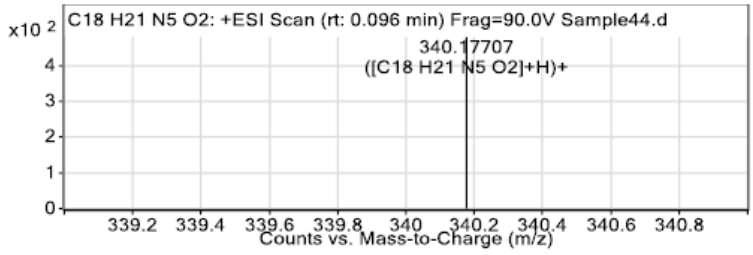

Peak List

m/z	z	Abund
100.01216		716
101.00172		758.46
102.12696		2935.24
125.98556		819.45
130.15831		1208.29
167.01174		868.47
185.11372	1	2942.39
362.15579	1	2343.85
378.1331		684.14
406.32531	1	1478.49

Formula Calculator Element Limits

Element	Min	Max
C	3	18
H	0	21
N	0	5
O	0	2

Formula Calculator Results

Formula	Best	Mass	Tgt Mass	Diff (ppm)	Ion Species	Score
C18 H21 N5 O2	DOGRU	339.16979	339.16952	-0.8	C18 H22 N5 O2	47.39

Data Sheet 2. HRMS data of S_2-TP

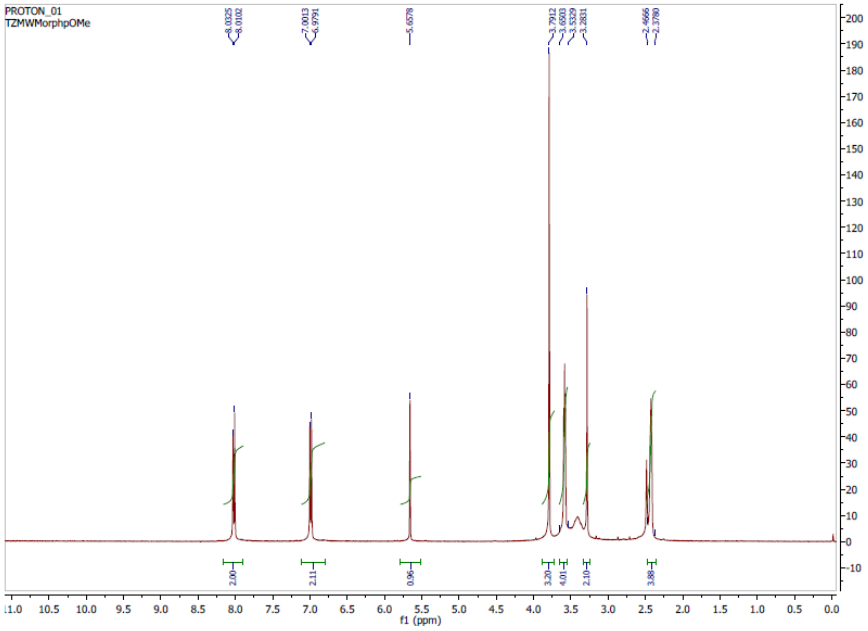

Supplementary Figure 5. ^{1}H NMR spectrum of S_3-TP

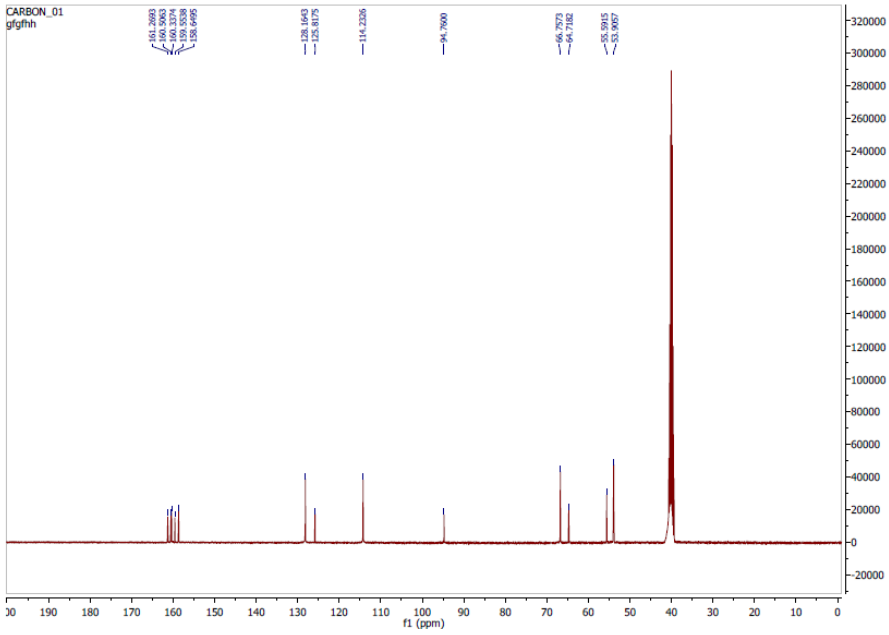

Supplementary Figure 6. ^{13}C NMR spectrum of S_3-TP

User Spectra

Fragmentor Voltage	Collision Energy	Ionization Mode
90	0	ESI

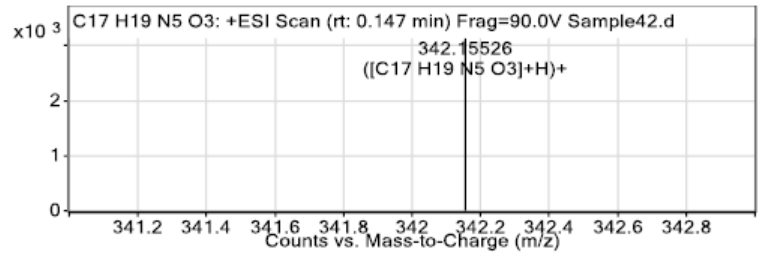

Peak List

m/z	z	Abund	Formula	Ion
132.90359		4762.14		
210.91546		1435.13		
342.15526	1	3130.95	C17 H19 N5 O3	(M+H)+
474.05149	1	16621.97		
474.10335		1299.25		
475.05505	1	2978.97		
547.10823	1	1285		
605.94806	1	4872.07		
683.30168	1	1764.2		
815.19928	1	3132.83		

Formula Calculator Element Limits

Element	Min	Max
C	3	17
H	0	19
N	0	5
O	0	3

Formula Calculator Results

Formula	Best	Mass	Tgt Mass	Diff (ppm)	Ion Species	Score
C17 H19 N5 O3	DOĞRU	341.14814	341.14879	1.89	C17 H20 N5 O3	83.48

Data Sheet 3. HRMS data of S_3-TP